Electronic Supplementary Material (ESI) for Physical Chemistry Chemical Physics.

Supporting information:

Ultrafast hydrogen production in boron/oxygen-codoped graphitic carbon nitride revealed by nonadiabatic dynamics simulations

Huijuan Yang,† Rongliang Wu,† Wei Li,‡ and Jin Wen*,†

†*State Key Laboratory for Modification of Chemical Fibers and Polymer Materials, College of Materials Science and Engineering, Donghua University, Shanghai 201620, China*

‡*Key Laboratory of Mesoscopic Chemistry of Ministry of Education, Institute of Theoretical and Computational Chemistry, School of Chemistry and Chemical Engineering, Nanjing University, Nanjing 210023, China*

E-mail: jinwen@dhu.edu.cn

Table of Contents

1. Doping scheme and formation energies 3
2. Band structure 8
3. The NAC and the pure dephasing time 9
4. Absorption spectra and vertical excitations 10
5. The optimized geometries and molecular orbitals 12
6. Representative trajectories and time-resolved evolution of bond lengths 13

1. Doping scheme and formation energies

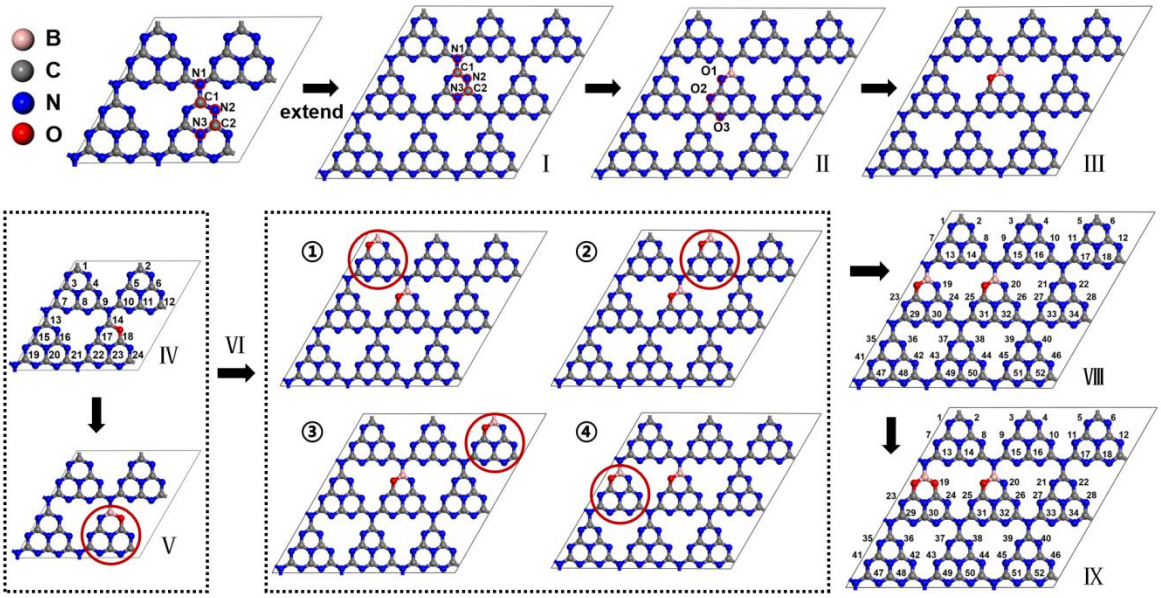

Figure S1. The doping scheme for B/O-GCN. According to the symmetry, positions of one boron and one oxygen atoms are determined from I-III models, with the formation energies listed in Table S1. Positions of the second boron and oxygen atoms are determined in models VI with the highlighted red circles. Positions of the rest two oxygens are determined by comparison of formation energies in VIII and IX provided in Tables S2 and S3 respectively.

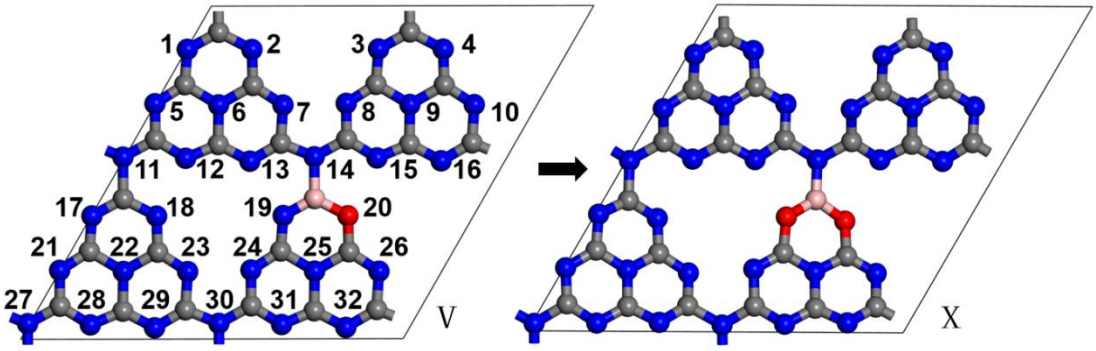

Figure S2. O substitutes the N doping positions in model V to obtain model X, which conforms to the experimental doping conditions, with the formation energies listed in Table S4.

Table S1. Formation energies, E_f in the unit of eV, in B-doped (I, IV), O-doped (II), and B/O-codoped (VI) models with different doping positions, which are depicted in Figure S1.

I	**N-rich**	**C-rich**	**II**	**N-rich**	**C-rich**	**VI**	**N-rich**	**C-rich**
C1	-3.28	-3.85	**O1**	-7.35	-7.49	①	-12.00	-12.29
C2	-3.23	-3.79	**O2**	-6.44	-6.58	②	-12.06	-12.34
N1	0.84	1.27	**O3**	-6.23	-6.37	③	-11.91	-12.19
N2	-2.45	-2.02				④	-12.08	-12.36
N3	-0.43	0.00						
Model IV								
1	-3.20	-3.34	**9**	-2.83	-2.97	**17**	-3.73	-3.87
2	-3.17	-3.32	**10**	-3.03	-3.17	**18**	-4.38	-4.52
3	-2.39	-2.53	**11**	-2.58	-2.72	**19**	-2.71	-2.86
4	-2.49	-2.63	**12**	-2.63	-2.77	**20**	-2.31	-2.45
5	-2.41	-2.56	**13**	-2.55	-2.69	**21**	-2.99	-3.13
6	-2.40	-2.54	**14**	-4.82	-4.96	**22**	-3.74	-3.88
7	-2.87	-3.01	**15**	-2.35	-2.49	**23**	-2.74	-2.88
8	-2.35	-2.49	**16**	-2.36	-2.51	**24**	-4.16	-4.30

Table S2. Formation energies, E_f in the unit of eV, in model VIII with different doping positions, which are depicted in Figure S1.

	Model VIII									
	N-rich	**C-rich**		**N-rich**	**C-rich**		**N-rich**	**C-rich**		**N-rich**	**C-rich**
1	-13.51	-13.37	**14**	-13.39	-13.25	**27**	-13.50	-13.36	**40**	-13.51	-13.36
2	-13.50	-13.36	**15**	-13.45	-13.31	**28**	-13.42	-13.28	**41**	-13.47	-13.33
3	-13.52	-13.38	**16**	-13.49	-13.34	**29**	-13.28	-13.13	**42**	-13.47	-13.33
4	-13.50	-13.35	**17**	-13.46	-13.32	**30**	-13.34	-13.20	**43**	-13.50	-13.36
5	-13.44	-13.30	**18**	-13.40	-13.25	**31**	-13.34	-13.20	**44**	-13.45	-13.31
6	-13.48	-13.34	**19**	-14.26	-14.12	**32**	-13.49	-13.35	**45**	-13.44	-13.30
7	-13.51	-13.37	**20**	-14.23	-14.09	**33**	-13.47	-13.33	**46**	-13.50	-13.36
8	-13.44	-13.30	**21**	-13.50	-13.36	**34**	-13.43	-13.28	**47**	-13.49	-13.35
9	-13.46	-13.32	**22**	-13.45	-13.31	**35**	-13.45	-13.31	**48**	-13.50	-13.36
10	-13.48	-13.34	**23**	-13.00	-12.86	**36**	-13.44	-13.30	**49**	-13.49	-13.35
11	-13.48	-13.34	**24**	-13.59	-13.45	**37**	-13.48	-13.34	**50**	-13.45	-13.31
12	-13.51	-13.37	**25**	-13.06	-12.92	**38**	-13.48	-13.34	**51**	-13.43	-13.29
13	-13.50	-13.36	**26**	-13.68	-13.54	**39**	275.21	275.35	**52**	-13.47	-13.33

Table S3. Formation energies, E_f in the unit of eV, in model IX with different doping positions, which are depicted in Figure S1.

	Model IX									
	N-rich	**C-rich**		**N-rich**	**C-rich**		**N-rich**	**C-rich**		**N-rich**	**C-rich**
1	-14.97	-13.27	**14**	-14.76	-13.06	**27**	-14.98	-13.27	**40**	-15.00	-13.29
2	-15.01	-13.30	**15**	-14.93	-13.23	**28**	-14.90	-13.19	**41**	-14.96	-13.26
3	-14.99	-13.29	**16**	-14.96	-13.26	**29**	-15.06	-13.36	**42**	-14.96	-13.25
4	-14.98	-13.27	**17**	-14.92	-13.22	**30**	-15.22	-13.52	**43**	-15.02	-13.32
5	-14.94	-13.23	**18**	-14.85	-13.15	**31**	-14.91	-13.20	**44**	-14.99	-13.28
6	-14.94	-13.23	**19**	—	—	**32**	-15.03	-13.32	**45**	-14.94	-13.23
7	-14.95	-13.25	**20**	-15.70	-13.99	**33**	-14.95	-13.24	**46**	-14.98	-13.28
8	-14.91	-13.20	**21**	-14.99	-13.28	**34**	-14.92	-13.21	**47**	-14.99	-13.28
9	-14.95	-13.24	**22**	-14.91	-13.21	**35**	-14.96	-13.25	**48**	-14.98	-13.28
10	-14.97	-13.26	**23**	-14.72	-13.02	**36**	-14.96	-13.25	**49**	-15.01	-13.31
11	-14.99	-13.29	**24**	-14.70	-12.99	**37**	-15.06	-13.36	**50**	-15.00	-13.29
12	-14.99	-13.29	**25**	-14.55	-12.85	**38**	-15.08	-13.38	**51**	-14.92	-13.22
13	-14.76	-13.06	**26**	-15.22	-13.51	**39**	268.23	269.94	**52**	-14.94	-13.24

Table S4. Formation energies, E_f in the unit of eV, in model V with different doping positions, which are depicted in Figure S2.

	Model V							
	N-rich	**C-rich**		**N-rich**	**C-rich**		**N-rich**	**C-rich**
1	-6.51	-5.90	**12**	-6.55	-5.95	**23**	-6.59	-5.98
2	-6.49	-5.88	**13**	-6.52	-5.91	**24**	-6.68	-6.07
3	-6.59	-5.98	**14**	—	—	**25**	—	—
4	-6.46	-5.86	**15**	-6.47	-5.86	**26**	-6.21	-5.60
5	-6.56	-5.95	**16**	-6.48	-5.88	**27**	—	—
6	—	—	**17**	-6.48	-5.87	**28**	-6.47	-5.87
7	-6.50	-5.89	**18**	-6.55	-5.95	**29**	-6.55	-5.94
8	-6.62	-6.02	**19**	-7.32	-6.71	**30**	—	—
9	—	—	**20**	—	—	**31**	-6.40	-5.80
10	-6.46	-5.85	**21**	-6.44	-5.83	**32**	-6.38	-5.77
11	—	—	**22**	—	—			

2. Band structure

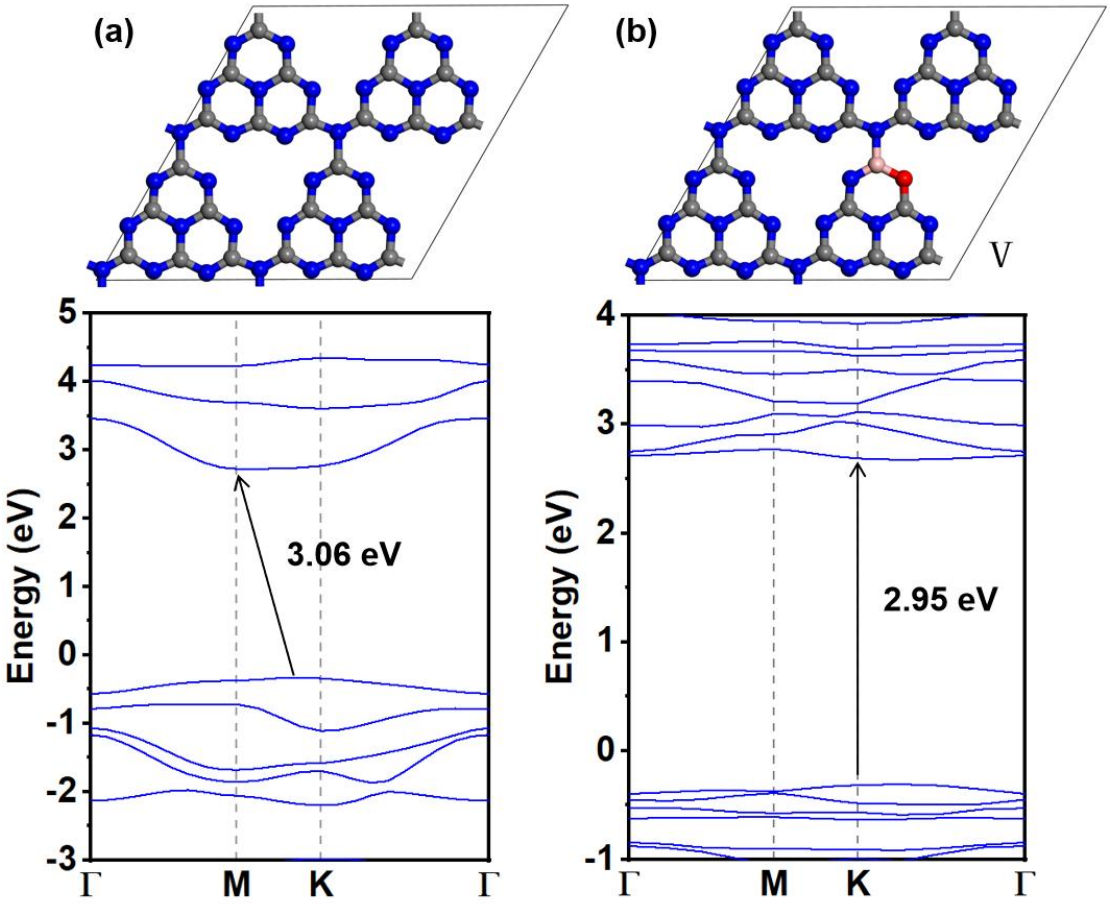

Figure S3. The electronic band structures in (a) GCN, and in the 2 × 2 × 1 supercell for (b) BO-GCN (model V) systems were obtained at the HSE06 level.

3. The NAC and the pure dephasing time

Table S5. Nonadiabatic coupling (NAC) in the unit of meV, pure dephasing time in the unit of fs, and recombination times in the unit of ns for GCN, BO-GCN and BO2-GCN systems.

VBM-CBM	NAC (meV)	Dephasing time (fs)	Recombination (ns)
GCN	0.60	5.75	17.97
BO-GCN	0.60	5.23	20.93
BO2-GCN	0.46	4.95	29.43

4. Absorption spectra and vertical excitations

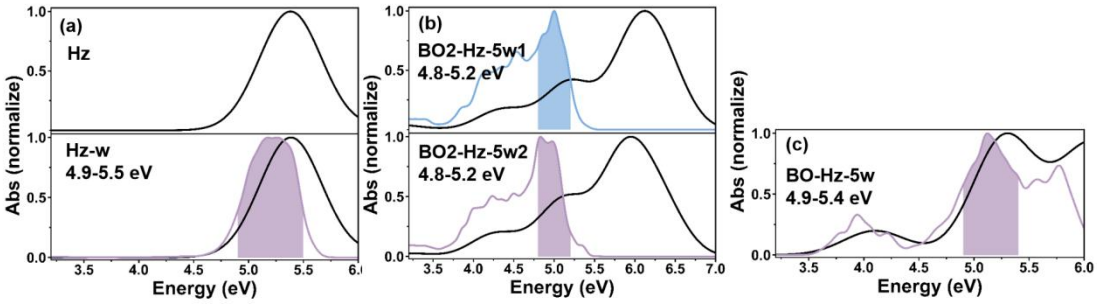

Figure S4. Simulated absorption spectra in black lines for (a) Hz, Hz-w, (b) BO2-Hz-5w (BO2-Hz-5w1 and BO2-Hz-5w2) and (c) BO-Hz-5w systems, convolved with a 0.67 eV FWHM Gaussian function. The shaded region signifies the energy window for the initial conditions sampled in excited-state dynamics simulations, convolved with a 0.10 eV FWHM Gaussian function, while the energy windows are listed in the insets.

Table S6. Vertical excitation energies (*E*) in electronvolts (eV) and oscillator strengths (*f*) (in parentheses) for the lowest ten excited states of the Hz-w, BO-Hz-w, and BO2-Hz-w systems.

	Hz-w	BO-Hz-w1	BO-Hz-w2	BO-Hz-w3		BO2-Hz-w1	BO2-Hz-w2
state	*E* (*f*)	*E* (*f*)	*E* (*f*)	*E* (*f*)	state	*E* (*f*)	*E* (*f*)
S_1	3.25 (ππ*) (0.0001)	4.06 (ππ*) (0.0678)	4.07 (ππ*) (0.0687)	4.07 (nπ*) (0.0585)	D_1	1.21 (nπ*) (0.0077)	1.25 (ππ*) (0.0065)
S_2	4.26 (nπ*) (0.0000)	4.21 (nπ*) (0.0002)	4.31 (nπ*) (0.0001)	4.28 (nπ*) (0.0002)	D_2	2.95 (nπ*) (0.0128)	2.60 (ππ*) (0.0177)
S_3	4.36 (nπ*) (0.0000)	4.46 (nπ*) (0.0002)	4.53 (nπ*) (0.0003)	4.50 (nπ*) (0.0003)	D_3	4.30 (nπ*) (0.0279)	4.29 (ππ*) (0.0142)
S_4	4.36 (nπ*) (0.0000)	4.63 (nπ*) (0.0002)	4.65 (nπ*) (0.0000)	4.64 (nπ*) (0.0001)	D_4	4.39 (nπ*) (0.0001)	4.40 (ππ*) (0.0000)
S_5	5.07 (nπ*) (0.0004)	5.23 (nπ*) (0.0017)	5.04 (CT) (0.0003)	5.15 (CT) (0.0001)	D_5	4.57 (ππ*) (0.0004)	4.58 (CT) (0.0351)
S_6	5.23 (nπ*) (0.0025)	5.25 (CT) (0.2769)	5.25 (nπ*) (0.0013)	5.19 (nπ*) (0.0008)	D_6	4.71 (nπ*) (0.0025)	4.61 (nπ*) (0.0022)
S_7	5.38 (CT) (0.3150)	5.33 (nπ*) (0.0000)	5.31 (nπ*) (0.3010)	5.27 (nπ*) (0.3127)	D_7	4.75 (nπ*) (0.0005)	4.72 (ππ*) (0.0022)
S_8	5.39 (CT) (0.3492)	5.64 (nπ*) (0.0002)	5.39 (nπ*) (0.0004)	5.38 (nπ*) (0.0004)	D_8	4.76 (nσ*) (0.0180)	4.77 (nπ*) (0.0000)
S_9	5.41 (nπ*) (0.0017)	5.81 (nπ*) (0.0003)	5.61 (nπ*) (0.0001)	5.67 (nπ*) (0.0001)	D_9	4.87 (nπ*) (0.0005)	5.04 (CT) (0.0069)
S_{10}	5.51 (nπ*) (0.0000)	5.82 (nπ*) (0.0002)	5.77 (ππ*) (0.0022)	5.87 (nπ*) (0.0000)	D_{10}	5.20 (ππ*) (0.0758)	5.20 (nπ*) (0.0022)

5. The optimized geometries and molecular orbitals

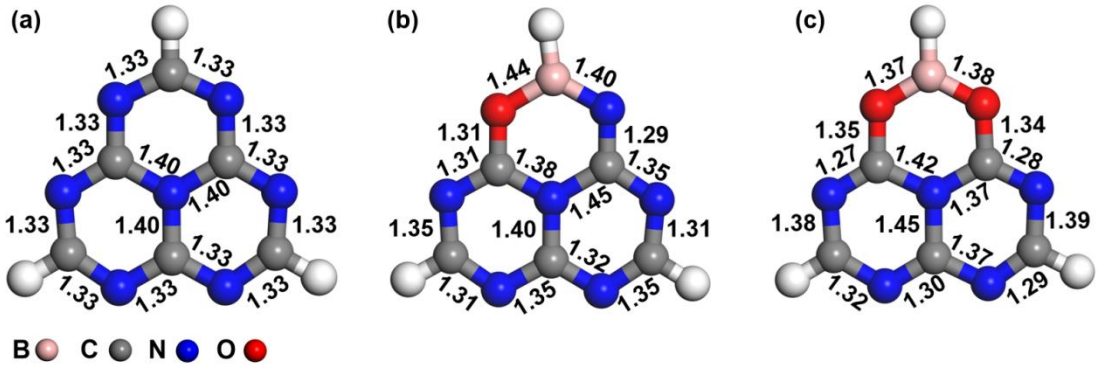

Figure S5. The optimized geometries of (a) Hz, (b) BO-Hz, and (c) BO2-Hz systems with the bond lengths listed in the unit of angstroms.

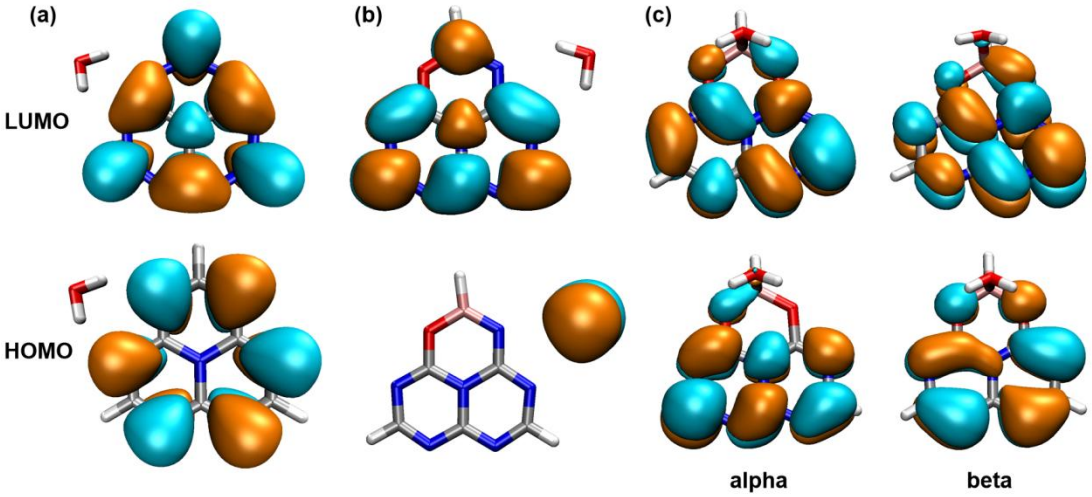

Figure S6. Molecular orbitals in (a) Hz-w, (b) BO-Hz-w2, and (c) BO2-Hz-w1 systems.

6. Representative trajectories and time-resolved evolution of bond lengths

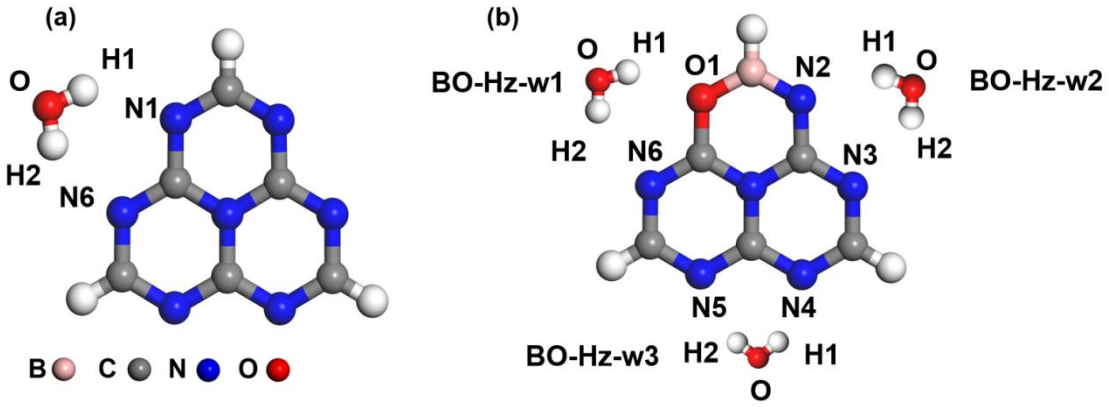

Figure S7. Atom numbering of the (a) Hz-w and (b) BO-Hz systems with different water positions labeled as w1-w3.

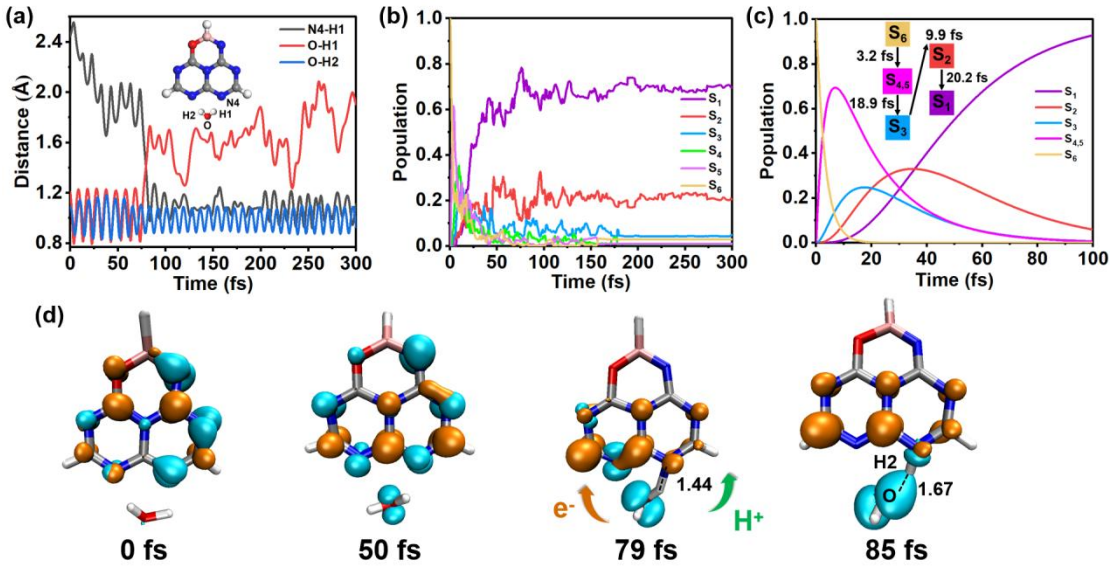

Figure S8. Representative trajectory illustrating a PCET reaction in the BO-Hz-w3 system over 300 fs. Time evolution in bond lengths between the water molecule and BO-Hz (a), and state populations with dynamics initiated in the S_6 state (b). (c) The kinetic model fits within 100 fs (insert: the time constants for the relaxation processes). (d) Charge density difference distributions in an activated state with an isosurface value set to 0.005. The negative and positive charges are presented in orange and blue respectively. The orange and green arrows represent electron and proton transfer respectively with the bond length listed in angstroms.

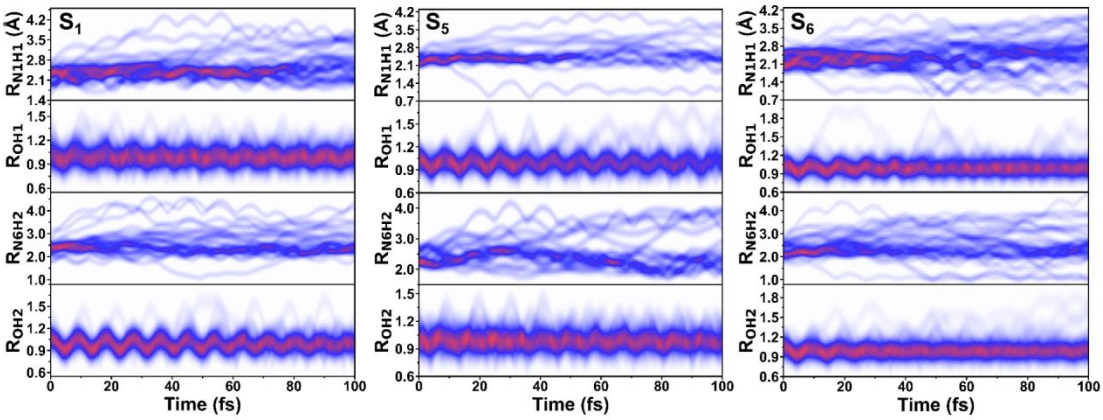

Figure S9. Time-resolved evolution of bond lengths for the Hz-w system in the S_1, S_5, and S_6 states, with simulated trajectories and PCET reaction probabilities (in parentheses) within 100 fs: 26 (0.00%) in S_1, 19 (5.30%) in S_5, and 36 (19.40%) in S_6.

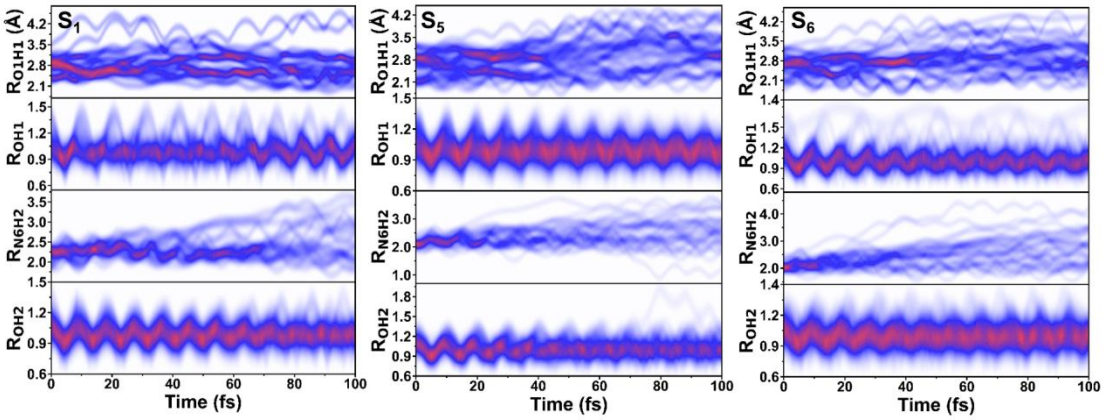

Figure S10. Time-resolved evolution of bond lengths for the BO-Hz-w1 system in the S_1, S_5, and S_6 states, with simulated trajectories and PCET reaction probabilities (in parentheses) within 100 fs: 18 (0.00%) in S_1, 31 (3.23%) in S_5, and 32 (0.00%) in S_6.

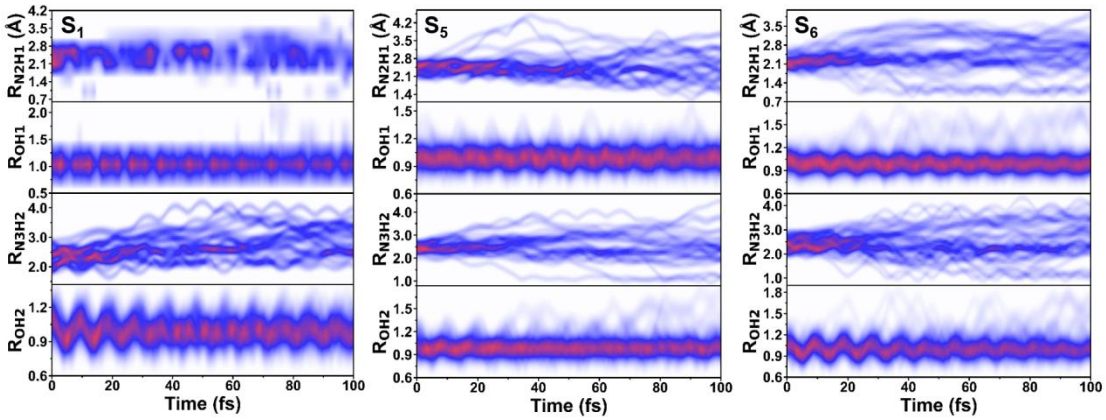

Figure S11. Time-resolved evolution of bond lengths for the BO-Hz-w2 system in the S_1, S_5, and S_6 state, with simulated trajectories and PCET reaction probabilities (in parentheses) within 100 fs: 18 (5.60%) in S_1, 26 (11.54%) in S_5, and 37 (27.03%) in S_6.

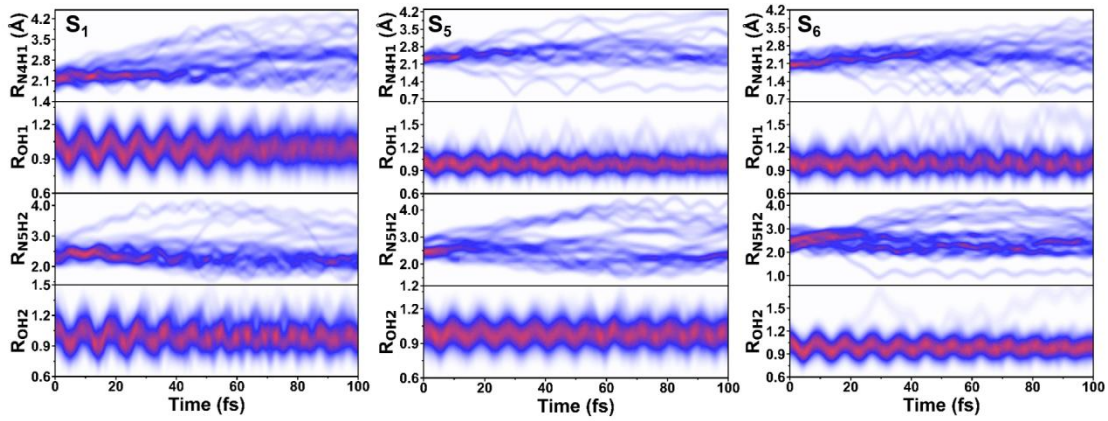

Figure S12. Time-resolved evolution of bond lengths for the BO-Hz-w3 system in the S_1, S_5, and S_6 state, with simulated trajectories and PCET reaction probabilities (in parentheses) within 100 fs: 30 (0.00%) in S_1, 20 (10.00%) in S_5, and 29 (20.69%) in S_6.

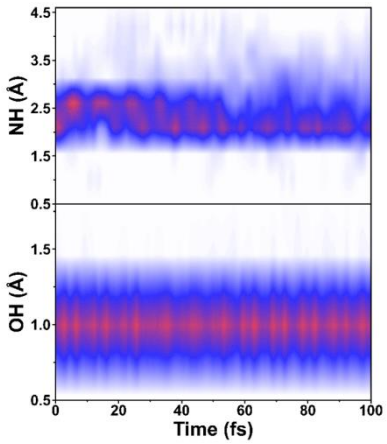

Figure S13. Time-resolved evolution of N-H and corresponding O-H bond lengths for the Hz-w, BO-Hz-w1, BO-Hz-w2, and BO-Hz-w3 systems in S_1.

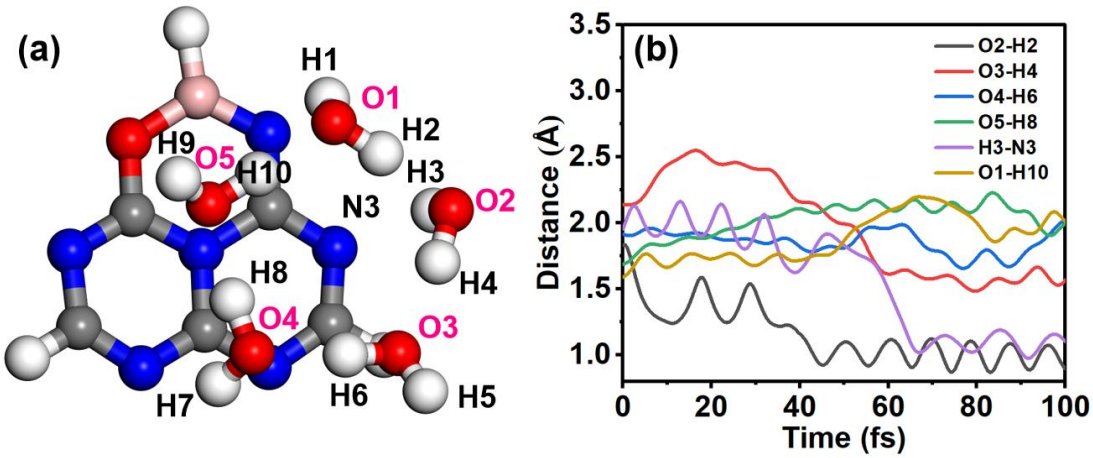

Figure S14. Representative trajectories initiated in the S_5 state of the BO-Hz-5w system. (a) The optimized geometry and atom numbering. (b) The time evolution of bond lengths.

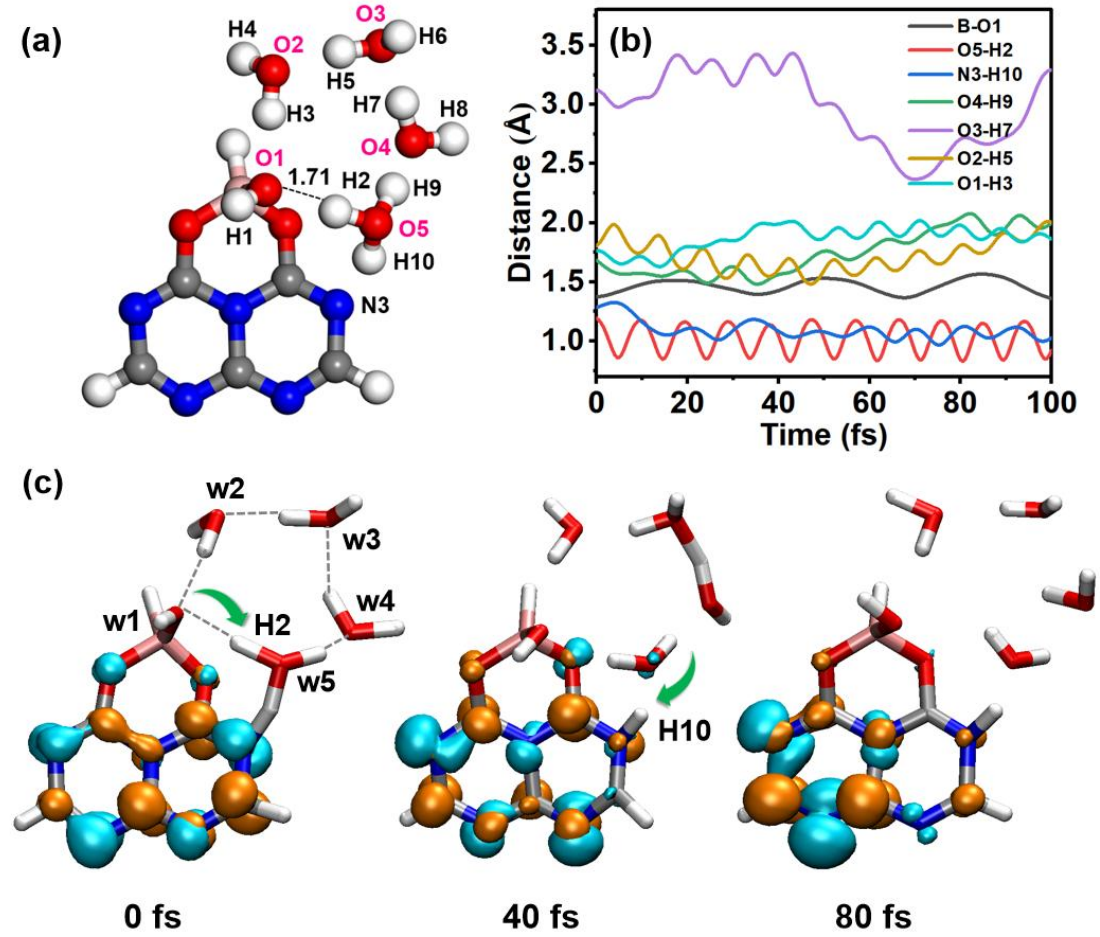

Figure S15. Representative trajectories in BO2-Hz-5w2. (a) The optimized geometry and atom numbering. (b) The time evolution of bond lengths in (b), accompanied by the corresponding charge density difference distributions depicted in (c). The dashed gray lines represent hydrogen bonds, while the green arrow indicates the direction of proton transfer.